Physica Medica 123 (2024) 103395

Contents lists available at ScienceDirect

Physica Medica

journal homepage: www.elsevier.com/locate/ejmp

Design and implementation of continuous bed motion (CBM) in Xtrim preclinical PET scanner for whole-body Imaging: MC simulation and experimental measurements

Bahador Bahadorzadeh [a,b], Reza Faghihi [a,c,*], Sedigheh Sina [a,c], Ahdiyeh Aghaz [d], Arman Rahmim [e,f], Mohammad Reza Ay [b,g]

[a] Nuclear Engineering Department, School of Mechanical Engineering, Shiraz University, Shiraz, Iran
[b] Research Center for Molecular and Cellular Imaging (RCMCI), Advanced Medical Technologies and Equipment Institute (AMTEI), Tehran University of Medical Sciences, Tehran, Iran
[c] Radiation Research Center (RRC), Shiraz University, Shiraz, Iran
[d] Radiation Application Research School, Nuclear Science and Technology Research Institute, Tehran, Iran
[e] Departments of Radiology and Physics Vancouver, The University of British Columbia, Vancouver, Canada
[f] Department of Integrative Oncology, BC Cancer Research Institute, Vancouver, Canada
[g] Department of Medical Physics and Biomedical Engineering, School of Medicine, Tehran University of Medical Sciences, Tehran, Iran

ARTICLE INFO

Keywords:
Preclinical PET
Continuous bed motion
Whole-body imaging
NEMA measurements

ABSTRACT

Purpose: Preclinical PET scanners often have limited axial field-of-view for whole-body (WB) scanning of the small-animal. Step-and-shoot(S&S) acquisition mode requires multiple bed positions (BPs) to cover the scan length. Alternatively, in Continuous Bed Motion(CBM) mode, data acquisition is performed while the bed is continuously moving. In this study, to reduce acquisition time and enhance image quality, the CBM acquisition protocol was optimized and implemented on the Xtrim-PET preclinical scanner for WB imaging.
Methods: The over-scan percentage(OS%) in CBM mode was optimized by Monte Carlo simulation. Bed movement speed was optimized considering ranges from 0.1 to 2.0 mm s^{-1}, and absolute system sensitivities with the optimal OS% were calculated. The performance of the scanner in CBM mode was measured, and compared with S&S mode based on the NEMA-NU4 standard.
Results: The optimal trade-off between absolute sensitivity and uniformity of sensitivity profile was achieved at OS-50 %. In comparison to S&S mode with maximum ring differences (MRD) of 9 and 23, the calculated equivalent speeds in CBM(OS-50 %) mode were 0.3 and 0.14 mm s^{-1}, respectively. In terms of data acquisition with equal sensitivity in both CBM(OS-50 %) and S&S(MRD-9) modes, the total scan time in CBM mode decreased by 25.9 %, 47.7 %, 54.7 %, and 58.2 % for scan lengths of 1 to 4 BPs, respectively.
Conclusion: The CBM mode enhances WB PET scans for small-animals, offering rapid data acquisition, high system sensitivity, and uniform axial sensitivity, leading to improved image quality. Its efficiency and customizable scan length and bed speed make it a superior alternative.

1. Introduction

Preclinical positron emission tomography (PET) imaging enables non-invasive study of molecular and physiological processes in small animal models [1]. Whole-body (WB) PET scans offer comprehensive assessment, but current preclinical scanners have a limited axial field-of-view [2,3]. To address this, step-and-shoot (S&S) data acquisition mode is employed for WB imaging, covering the entirety of small animals across multiple bed positions [4]. PET scans employing continuous bed motion (CBM) acquisition mode offer efficient whole-body (WB) imaging without imaging gaps or prolonged scan times [5,6]. This technique utilizes specialized detectors and motion correction algorithms to maintain image quality [7,8]. CBM acquisitions allow for flexible and optimized protocols for extended or WB scans, reducing scan durations and increasing optimization capabilities [9]. In dynamic PET protocols, CBM mode offers increased flexibility, particularly in sequential bi-

* Corresponding author at: Department of Nuclear Engineering, School of Mechanical Engineering, Shiraz University, Shiraz, Iran
E-mail address: faghihir@shirazu.ac.ir (R. Faghihi).

https://doi.org/10.1016/j.ejmp.2024.103395
Received 27 November 2023; Received in revised form 9 May 2024; Accepted 1 June 2024
Available online 5 June 2024

directional scanning. Unlike S&S techniques prone to issues like overlapping bed positions, CBM mode simplifies workflow and eliminates such problems, as demonstrated in recent clinical studies [10,11].

The objective of this study is to reduce acquisition time and enhance image quality in multiple BPs scans, by optimizing the over-scan percentage and bed speed in the CBM acquisition mode via Monte Carlo (MC) simulation. These considerations took into account the sensitivity of coincidence count rate detection and image quality. Subsequently, the CBM mode was implemented on the Xtrim preclinical PET scanner for static and dynamic WB imaging. The performance evaluation of the Xtrim-PET scanner with the implemented CBM acquisition mode was measured based on the National Electrical Manufacturers Association (NEMA) standard [12] and compared with the S&S mode.

2. Methods

2.1. Monte Carlo simulation and CBM optimization

2.1.1. Xtrim preclinical PET scanner

The Xtrim-PET scanner consists of ten detector blocks, arranged as 24 crystal rings. Each detector block has a size of $50.3 \times 50.3\ mm^2$ and is coupled with a Silicon Photomultiplier (SiPM) that has an array size of 12×12 and a pixel pitch of 4.2 mm. These SiPMs (Sensl ArrayC-30035-144P-PCB, Onsemi Co., Semiconductor Components Industries, LLC, US) are connected to a pixelated LYSO: Ce scintillator (EPIC Crystal Co Ltd, Jiangsu, China), which is responsible for capturing the scintillation light. Each detector block comprises 24×24 crystal elements, totalling 576 crystals per block. Each crystal element has a cross-section measuring $2 \times 2\ mm^2$ with a thickness of 10 mm. Fig. 1 displays the model of the entire scanner, the simulated geometry of the Xtrim-PET, and the phantoms utilized, which include the mouse-like, rat-like, and IQ Phantom.

2.1.2. Simulation and validation

For optimization purposes, this study implemented a research approach that involved conducting a computer simulation using the Geant4 Application for Tomographic Emission (GATE) MC code [15]. To validate the simulation model of the Xtrim-PET scanner, the NEMA NU4-2008 standard was selected as the benchmark for comparison [12]. The pixel pitch of each crystal element is 2.1 mm. A reflector material made of barium sulphate (BaSO4) with a thickness of 0.1 mm was utilized between the LYSO segments. The AFOV is 50 mm, while the transaxial field-of-view (TFOV) is 100 mm [13,14].

2.1.3. Continuous bed motion (CBM) acquisition mode

In CBM acquisition mode, "Over-Scan" (OS) refers to the bed's position relative to the AFOV, indicating the percentage of AFOV covered at the scan's start and end [16]. Using MC simulation to optimize OS% in CBM mode, factors like system sensitivity, scan length, and scan time in S&S mode were considered, leading to a chosen constant speed of 0.15 s^{-1}. In the S&S mode, the scan time for a single bed position is approximately 5–6 min. To achieve the same scan time in both data acquisition modes, the bed speed in CBM mode should be set to the speed mentioned earlier. The absolute system sensitivity in CBM mode was evaluated for four OS positions: 25 %, 50 %, 75 %, and 100 %. The simulations were performed using identical scan times, without the applying of the maximum ring difference (MRD), and with a scan length equal to the size of the AFOV. Additionally, to optimize the OS% for different scan lengths in CBM mode, the absolute system sensitivities were evaluated for scan lengths equal to 2, 3, and 4-BPs in S&S mode, specifically for WB imaging of mice and rats (Fig. 2). To compare the absolute sensitivity, the scan lengths were kept the same due to the 21 % axial overlap in multiple BPs in S&S mode. For a single BP, the calculation of the absolute sensitivity profile was performed, considering a scan length equal to the AFOV of the scanner (50.4 mm). Additionally, absolute sensitivity profiles were calculated for scan lengths equal to 2,

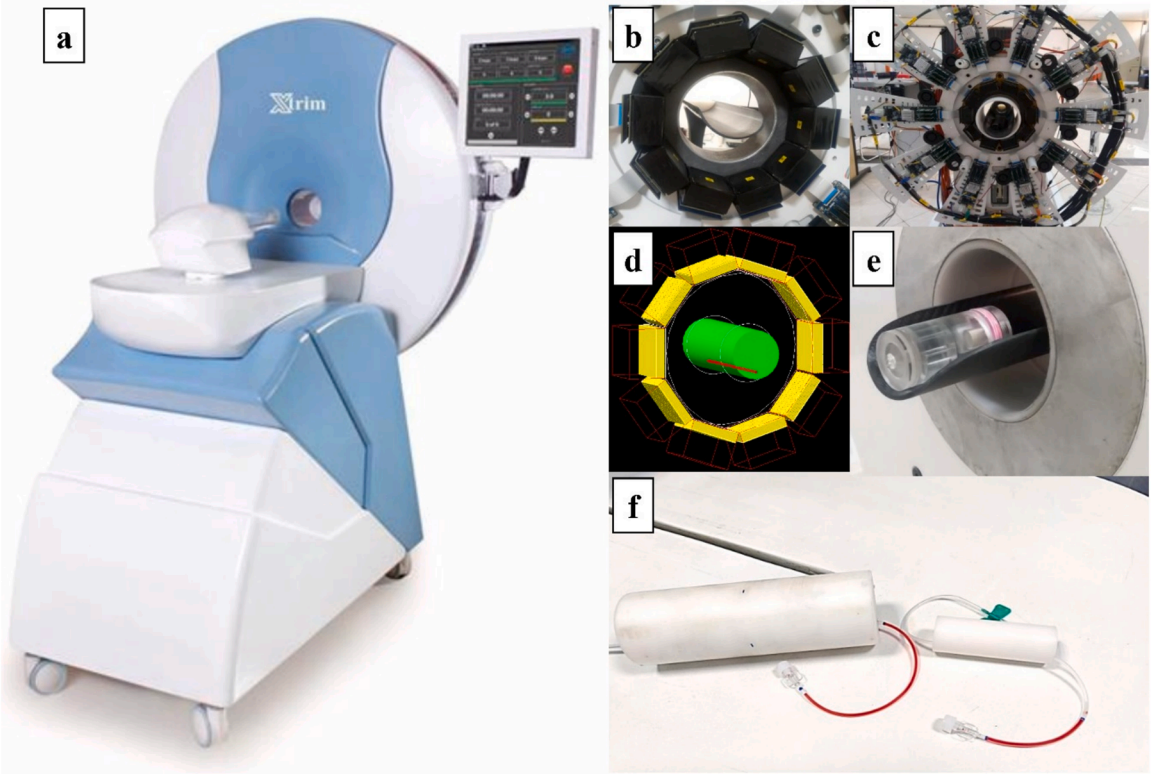

Fig. 1. The visual display of the Xtrim-PET scanner with a ring diameter of 160.8 mm (a), the arrangement of blocks (b), gantry (c), a graphic representation of the MC simulated scanner model (d), the IQ phantom (e), and the mouse-like and rat-like phantoms (f).

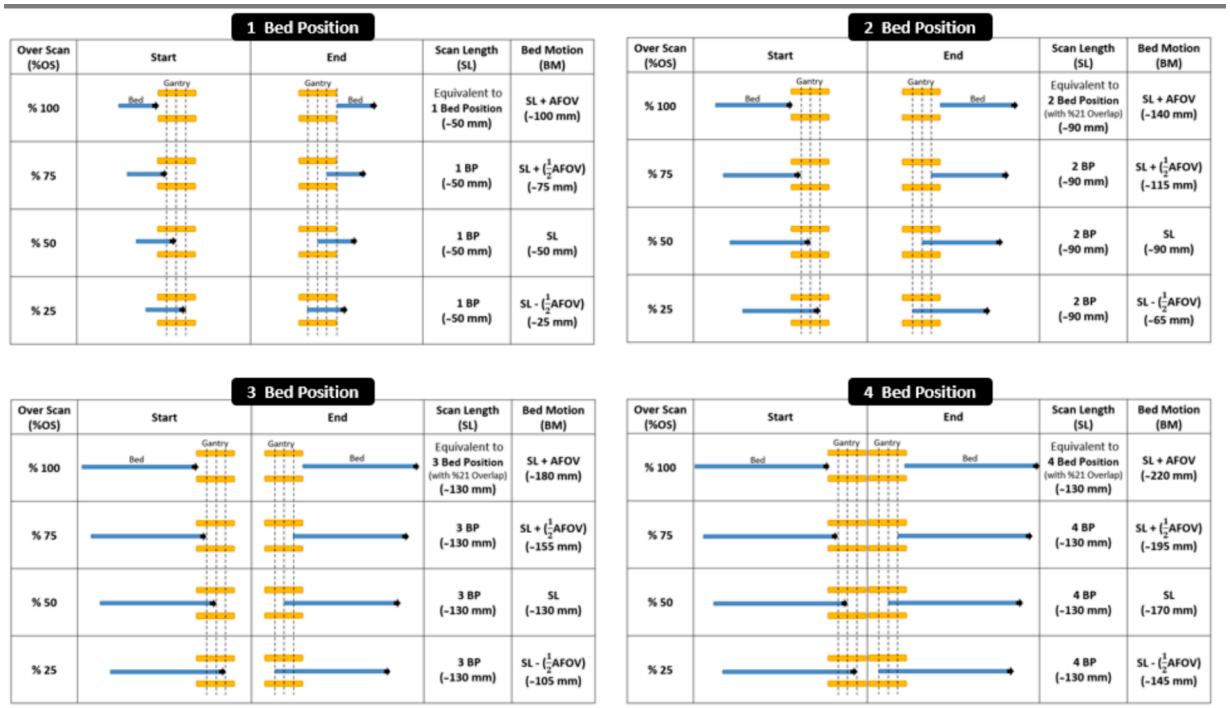

Fig. 2. The position of the start and the end of the bed movement in CBM mode for different OS% for the scan lengths equal to 1, 2, 3, and 4-BPs in S&S mode (%21 overlap in multiple bed positions).

3, and 4-bed positions (90.3 mm, 130.2 mm, and 170.1 mm, respectively).

To identify the optimal OS%, the OS values with high total absolute system sensitivities were initially selected. Subsequently, an analysis of the sensitivity profiles along the axial axis was performed to identify the optimal OS% among these high absolute sensitivity values. The analysis focused on the coefficient of variation (CV) to measure sensitivity profile uniformity. To determine the optimal speed for bed movement (BM), various speeds ranging from 0.1 to 2.0 mm s^{-1} were assessed. The absolute system sensitivities were calculated for each speed, considering the optimal OS% for scan lengths of 1, 2, 3, and 4 BPs.

2.2. Performance measurement: NEMA NU-4 standard

A comprehensive performance evaluation based on the NEMA NU-4 standard for both acquisition modes was performed [12], which included the determination of spatial resolution, sensitivity, count rate performance, scatter fraction (SF), and image quality. To evaluate the spatial resolution and system sensitivity, a cylindrical source with a height of 1 ± 0.2 mm and a diameter of 1 mm was uniformly filled with 1.85 ± 1 MBq (50 ± 3 μCi) ^{18}F. Sinograms were reconstructed using filtered back-projection (FBP) with a slice thickness of 1.05 mm and a pixel grid size of 0.33 × 0.33 mm^2. To evaluate the NECR and the scatter fraction (SF), a line sources containing ^{18}F water solution with activity concentrations of 0.85 ± 0.04 MBq cc^{-1} and 0.19 ± 0.01 MBq cc^{-1} were inserted into the holes of the mouse-like and rat-like phantoms, respectively. To evaluate the image quality in both S&S and CBM acquisition modes, the image quality (IQ) phantom specified in the NEMA NU4 was utilized. The IQ phantom was filled with a 3.7 ± 2 MBq (100 ± 5 μCi) ^{18}F aqueous solution, and data was acquired. The uniformity, recovery and coefficients (RCs), and spill-over ratios (SORs) were assessed and reported following the NEMA NU4 standard. To measure the activity of point sources prepared using capillary tubes and the activity of line sources within the mouse-like and rat-like phantoms, the PTW CURIEMENTOR® 3 Dose Calibrator was utilized, which offers an accuracy reading of ± 5.5 %. Additionally, the correction factors for the reading values of the point and line sources used in this study were calculated and applied.

2.3. S&S vs. CBM for static and dynamic WB imaging

The sensitivity values were compared for multiple BPs for static WB imaging in both S&S and CBM modes, considering a fixed scan time. Additionally, the scan times were compared, assuming the same sensitivity for both modes. Subsequently, the absolute system sensitivity and scan time were compared for dynamic WB imaging in both modes, considering different numbers of passes (N) and scan lengths of 90.3, 130.2, and 170.1 mm (2, 3, and 4BPs). A proposed protocol was presented for WB dynamic imaging in mice (70 mm) and rats (150 mm) using the optimal speed in CBM mode for various numbers of passes. In this protocol, the heart of the mouse or rat is initially scanned for a few minutes, corresponding to the WB scan time. This is followed by a bi-directional WB scan with N passes (e.g., N = 6). The constant bed speed in CBM mode is determined proportionally to the scan length and the total scan time required to achieve the same sensitivity as the S&S mode.

3. Results

3.1. MC simulation and CBM optimization

3.1.1. Simulation and validation

The results of the NEMA tests from both MC simulation and experimental measurement, including the spatial resolution, sensitivity, NECR, and SF presented, are as follows: *Spatial resolution:* The radial full width at half maximum (FWHM) values obtained at a radial distance of 5 mm from the CFOV were 1.96 ± 0.04 mm and 2.05 ± 0.11 mm for MC simulation and experimental measurement, respectively. Similarly, the tangential FWHM values were 1.90 ± 0.03 mm and 1.98 ± 0.12 mm, respectively. For various radial distances, the maximum difference between the spatial resolution values obtained from simulation and measurement was found to be 8 %. *Sensitivity:* The simulated peak absolute

sensitivity, utilizing a timing window of 5 ns, and an energy window of 250–650 keV, was found to be 3.14 ± 0.06 %, while the measured sensitivity was slightly lower at 3.02 ± 0.17 %. Additionally, it is worth noting that the simulated sensitivities at all axial offsets were consistently higher by approximately 4 to 6 % compared to the measured sensitivities. *NECR, and SF:* The simulated and measured peak NECRs for the mouse-like phantom at an activity concentration of 0.36 MBq cc^{-1} were determined to be 118.7 ± 2.4 kcps and 115.3 ± 6.9 kcps, respectively. Similarly, for the rat-like phantom at 50.1 kBq cc^{-1}, the simulated and measured peak NECRs were found to be 86.7 ± 1.7 kcps and 83.85 ± 4.6 kcps, respectively. The simulated and measured SFs for the mouse-like phantom were determined to be 12.2 ± 0.3 % and 13.1 ± 0.8 %, while for the rat-like phantom were found to be 25.1 ± 0.6 %, and 27.5 ± 1.7 %, respectively. The differences between the peak NECRs and SFs obtained from the simulated model and measured results were found to be 7 % and 9 %, respectively. The comparison between the MC simulation and experimental measurement demonstrates a close alignment between the measured data and the simulation results, indicating the validity of the simulation.

3.1.2. CBM data acquisition mode

Fig. 3 depicts the absolute sensitivity profiles of the Xtrim-PET scanner in the CBM acquisition mode, which were calculated using MC simulation. The absolute sensitivities are graphically represented as a function of axial offset for OS positions of 25 %, 50 %, 75 %, and 100 % in single-bed and multiple BPs (2, 3, and 4 BPs). The corresponding scan lengths are 50.4 mm, 90.3 mm, 130.2 mm, and 170.1 mm, respectively. The total absolute system sensitivities, denoted by the area under the sensitivity profiles (equation 2), for 1 BP in S&S mode, both with (MRD9) and without MRD (WO-MRD or MRD23), were 52.8 % and 79.1 % for 1 BP, respectively. In contrast, for the CBM mode, the total absolute system sensitivities at OS locations of 25 %, 50 %, 75 %, and 100 % were found to be 77.2 %, 66.5 %, 51.7 %, and 39.7 %, respectively. Table 1 presents the calculated total absolute system sensitivities with and without MRD for S&S mode, as well as the sensitivities for various OS% in CBM mode. Additionally, the table shows the variation of sensitivities across the axial direction for 1, 2, 3, and 4 BPs. In all cases, the sensitivity is quantified in counts per second per Becquerel (cps/Bq), while the absolute sensitivity is expressed as a dimensionless percentage. Furthermore, the absolute system sensitivities presented in this table correspond to the area under the sensitivity profiles, as computed by equation 2.

For data acquisition with the same total absolute system sensitivity in both CBM(OS-50 %) and CBM(WO-MRD) modes, the total scan time in CBM mode increases by 16.0 % for single-BP. However, for scan lengths of 2, 3, and 4 BPs, the total scan time in CBM(OS-50 %) mode exhibits a decrease of 1.9 %, 7.7 %, and 10.7 %, respectively. In contrast, when considering data acquisition with identical total absolute system sensitivity in CBM(OS-50 %) and S&S(MRD-9) modes, the total scan time in CBM mode demonstrates significant reductions. Specifically, for scan lengths of 1, 2, 3, and 4 BPs, the total scan time decreases by 25.9 %, 47.7 %, 54.7 %, and 58.2 %, respectively.

Fig. 4 presents the absolute sensitivity profile of the Xtrim-PET scanner, calculated for optimal OS percentages and scan lengths ranging from 1 to 4 BPs. The calculations were performed for various bed speeds, specifically 0.1, 0.15, 0.2, 0.4, 0.6, 0.8, 1.0, 1.5-, and 2.0 mm s^{-1}, in CBM mode. The mentioned speeds were evaluated in order to cover the maximum scanning time for static scanning (0.1 mm s^{-1} equivalent to 8.4 min BP^{-1}) and the minimum scanning time for scanning one pass in dynamic imaging (2 mm s^{-1} equivalent to 0.42 min BP^{-1}) with scan lengths equal to 1–4 BPs. The ratios of the CBM mode's total absolute system sensitivity with optimal OS (OS-50 %) for the bed speeds as mentioned earlier, relative to the CBM(WO-MRD) mode with a constant scan time of 336 sec BP^{-1} for a scan length of single-BP are as follows: 1.26, 0.84, 0.63, 0.32, 0.21, 0.16, 0.13, 0.08, and 0.06, respectively. In contrast, when comparing CBM mode to S&S(MRD-9) mode, these ratios are as follows: 1.89, 1.26, 0.94, 0.47, 0.31, 0.24, 0.19, 0.13, and 0.09, respectively.

Fig. 5 provides a graphical representation of the required speed in CBM(OS-50 %) mode to achieve an equal total absolute system

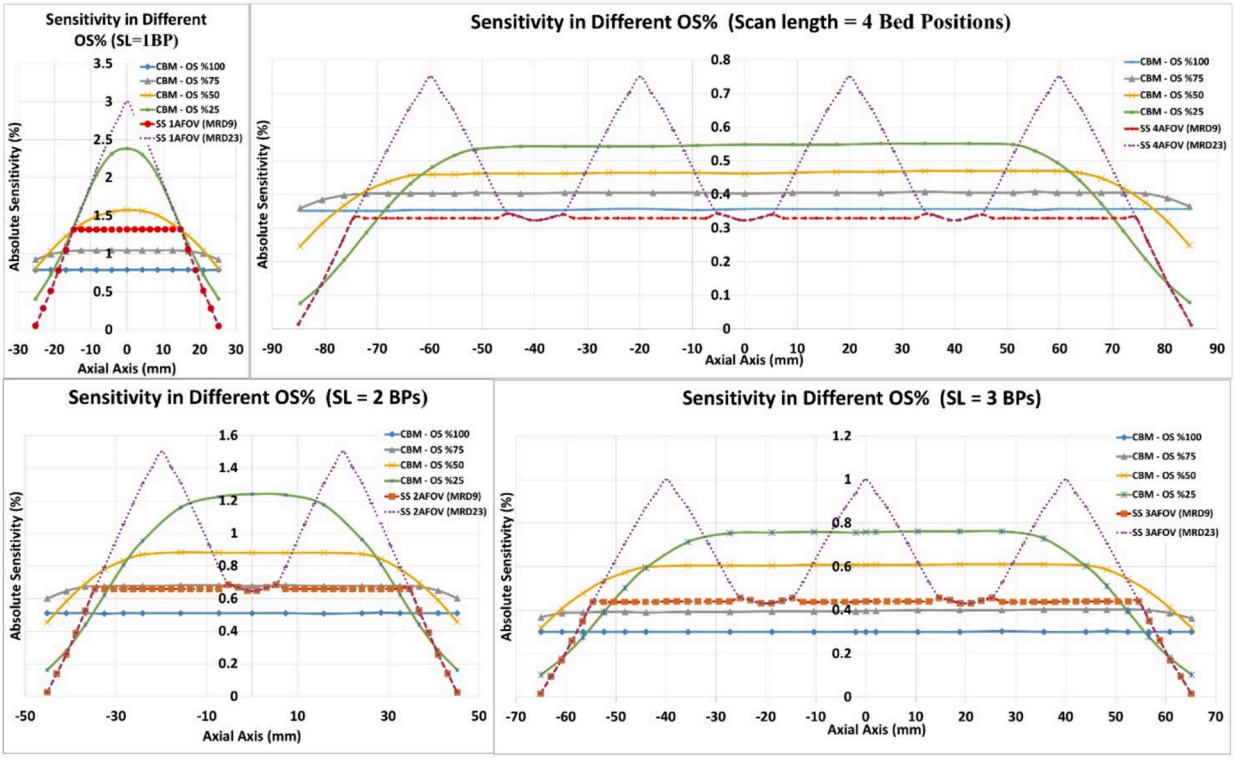

Fig. 3. The calculated absolute system sensitivity with different OS% positions in CBM mode, and with and without MRD in S&S mode.

Table 1
The calculated total absolute system sensitivities and the associated coefficient of variation (CV) profiles for different OS% in CBM mode. Furthermore, the calculated sensitivities for both with and without MRD in S&S mode for scan lengths ranging from 1 to 4 BPs.

Total Absolute System Sensitivity and CV								
OS	1 BP		2 BPs		3 BPs		4 BPs	
	Sensitivity (%)	CV (%)	Sensitivity (%)	CV (%)	Sensitivity (%)	CV (%)	Sensitivity (%)	CV (%)
25 %	77.17	49	78.96	52	79.21	45	79.03	39
50 %	66.46	21	72.42	19	74.28	17	75.25	15
75 %	51.72	4	60.68	4	51.42	3	68.22	3
100 %	39.71	1	46.11	1	39.09	1	60.20	1
S&S (MRD-9)	52.77	44	52.75	32	52.74	27	52.76	23
S&S (MRD-23)	79.10	61	79.15	48	79.17	43	79.18	40

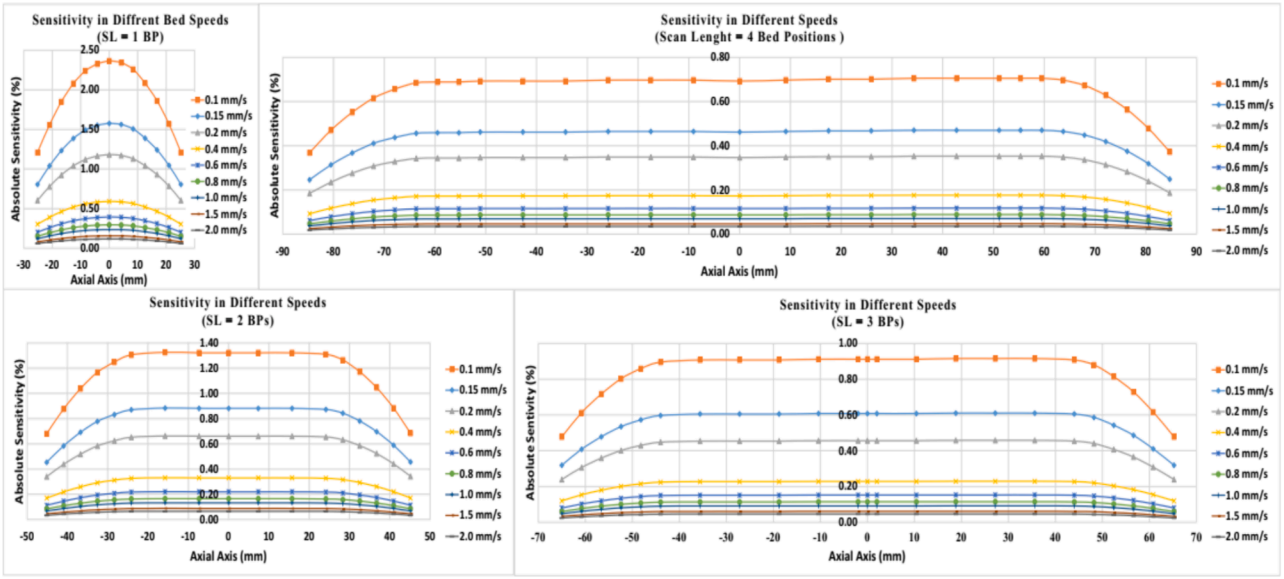

Fig. 4. The calculated absolute sensitivity profiles with optimal OS% for different bed speeds in CBM mode.

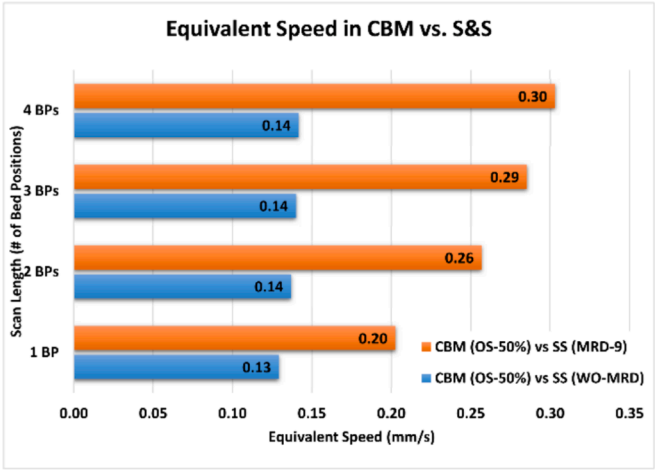

Fig. 5. The equivalent speed in CBM(OS-50%) mode versus CBM (with and without MRD) mode.

sensitivity for scan lengths ranging from 1 to 4 BPs in both data acquisition modes. In other words, the total absolute system sensitivity in S&S mode for scan lengths ranging from 1 to 4 BPs is equal to that achieved in CBM mode with the equivalent speed.

3.2. Performance measurements: NEMA NU-4 standard

The following are the results of the NEMA tests measuring CBM and S&S modes, which include spatial resolution, sensitivity, NECR, SF, and image quality.

3.2.1. Spatial resolution

In CBM mode, the measured FWHM values at a radial distance of 5 mm, were 1.95 mm and 1.98 mm for the radial, tangential directions, respectively. These values increased to 2.57 mm and 2.61 mm, respectively, at a radial distance of 25 mm. Notably, the measured axial FWHM exhibited a higher dependence on bed movement and radial distance, degrading from 2.02 mm to 3.19 mm as the radial distance increased from 5 mm to 25 mm. Furthermore, when comparing CBM(OS-50 %) and S&S(MRD-9) modes, the analysis revealed that the maximum difference in spatial resolution values was 3.3 % in the radial and tangential directions. However, in the axial direction, the maximum difference reached 10.4 %.

3.2.2. Sensitivity

The analysis revealed peak absolute sensitivities of 1.6 % for the CBM mode and 3.0 % for the CBM(WO-MRD) mode. Moreover, the total absolute system sensitivities, computed using Equation 2, were determined to be 64.8 % for CBM mode, 76.7 % for CBM(WO-MRD) mode, and 51.3 % for S&S(MRD-9) mode.

3.2.3. NECR and SF

A comparison was performed between the data acquisition in CBM

(OS-50 %) mode with a bed speed of 0.13 mm s^{-1} and S&S(MRD-9) mode, specifically for a single-PB scan length. The peak NECR values for the mouse-like phantom at an activity concentration of 360 kBq cc^{-1} were measured 117.8 kcps and 115.3 kcps in CBM and S&S modes, respectively. Similarly, for the rat-like phantom at 50.1 kBq cc^{-1}, the peak NECR values were measured 85.6 kcps and 83.8 kcps in CBM and S&S modes, respectively. The measured SF values for the mouse-like phantom were 12.8 % and 13.1 % in CBM and S&S modes, respectively. Additionally, for the rat-like phantom, the SF values were determined to be 26.4 % and 27.5 % in CBM and S&S modes, respectively.

3.2.4. Image quality

Table 2 summarized the measured uniformity values, RCs for rod sizes from 1 to 5 mm diameter, and SORs obtained from the IQ phantom images for both S&S(MRD-9) and CBM(OS-50 %) modes.

3.3. S&S mode versus CBM mode for static and dynamic WB imaging

The total absolute system sensitivities for 2, 3, and 4 BPs in CBM(OS-50 %) mode were calculated to be 72.42 %, 74.28 %, and 75.25 %, respectively. In contrast, the total absolute system sensitivities for all BPs in the S&S mode, both with and without MRD, were approximately 52.75 % and 79.15 %, respectively. The S&S mode has a scan time of 336 s for each BP, resulting in total scan times of 672 s, 1008 s, and 1344 s for 2, 3, and 4 BPs, respectively. Consequently, the total scan times required in CBM mode to achieve the same sensitivity to S&S(MRD-9) mode were calculated as 351 s, 456 s, and 561 s for 2, 3, and 4 BPs, respectively. In contrast, the total scan times in CBM mode required to reach the same sensitivity as CBM(WO-MRD) mode were calculated as 659 s, 930 s, and 1200 s for 2, 3, and 4 BPs, respectively. Fig. 6 illustrates a comprehensive comparison of scan times between CBM and S&S modes across a range of scan lengths from 1 to 4 BPs, based on achieving the same absolute system sensitivity in both modes.

A proposed protocol for WB dynamic imaging of mice (70 mm) and rats (150 mm) is outlined as follows: Initially, a short scan of the heart is performed for a few minutes (1.7, 2.5, and 3.3 min) for both mice and rats. This is followed by a bi-directional WB scan with multiple passes, denoted as N passes. The value of the constant bed speed in CBM mode is determined based on the equivalent speed. In CBM mode with the equivalent speed, the absolute system sensitivity for a given scan length equals a single whole-body scan in S&S mode, as explained in section 3.1.2. Therefore, to achieve the same absolute system sensitivity in both modes for a multi-pass CBM WB dynamic PET scan with N passes, the selected speed is multiplied by N. To provide a concrete example, in WB imaging of a mouse in CBM(OS-50 %) mode with a scan length equal to 2 BPs in S&S(MRD-9) mode, to achieve the same absolute system sensitivity in both modes, a bed speed of 0.26 mm s^{-1} is selected. Similarly, for dynamic whole-body imaging with 6 passes (N = 6) in CBM mode, a bed speed of approximately 1.5 mm s^{-1} is chosen. Likewise, in the case of WB imaging of a rat in CBM mode with a scan length equal to 4 BPs in S&S mode, a bed speed of 0.3 mm s^{-1} is selected to achieve the same absolute sensitivity in both modes. Furthermore, for dynamic WB imaging with 6 passes in CBM mode, a bed speed of 1.8 mm s^{-1} is chosen.

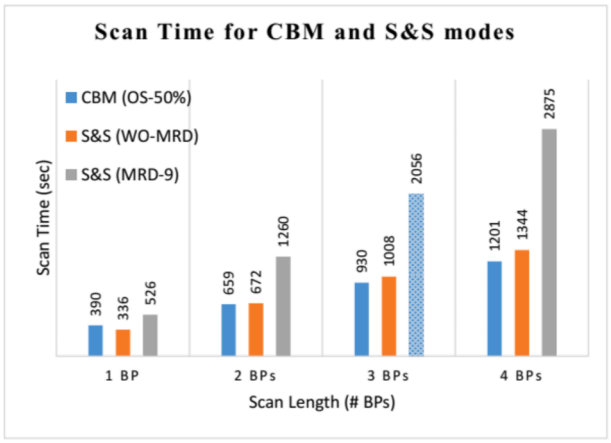

Fig. 6. The scan time in CBM(OS-50%) mode versus CBM (with and without MRD) mode for scan lengths of 1–4 BPs.

4. Discussion

Understanding system characteristics introduced by close geometry is crucial for optimizing data acquisition protocols and guiding system design in preclinical PET systems. Scan time reduction is key in whole-body imaging, where the technique of multiple BPs significantly impacts duration. This study optimizes CBM acquisition mode for multiple BPs scans using MC simulation and experimental validation. CBM mode was implemented on the Xtrim-PET system for whole-body scanning, focusing on absolute system sensitivity and image quality. Results can benefit other closed geometry PET systems using CBM. Xtrim-PET performance was evaluated following the NEMA NU4 2008 standard in simulation and measurement, showing good agreement, validating our methods and simulation model's precision and accuracy.

The optimal OS% in CBM mode depends on absolute system sensitivity and sensitivity profile uniformity. OS-25 % exhibits the highest absolute sensitivity for scan lengths of 1 to 4 BPs, while OS-100 % maintains a steady CV at 1 %. A clear trade-off exists between absolute sensitivity and the uniformity of the sensitivity profile. The absolute sensitivity for OS-25 % in CBM mode (77.2 %) is almost close to the absolute sensitivity in the S&S mode (79.1 %) without applying the MRD (WO-MRD or MRD-23). Given their impact on data acquisition and image quality, OS-25 % and OS-50 % were considered optimal, with OS-50 % having a substantially lower CV, indicating a more uniform sensitivity profile. Thus, OS-50 % was deemed optimal considering both absolute sensitivity and uniformity.

Table 1 and Fig. 3 present absolute sensitivity values and sensitivity profiles for S&S mode with various scan lengths (1–4 BPs). Applying MRD-9 decreases absolute sensitivity by 33.3 % compared to WO-MRD, ensuring uniform axial sensitivity. However, it sacrifices overall system sensitivity. In CBM mode with OS-50 %, absolute sensitivity increases by 26–43 % across scan lengths compared to S&S with MRD-9. CBM mode enhances axial sensitivity uniformity and reduces noise at scan start and end points. Despite a slight 11 % reduction in axial resolution, CBM mode maintains radial and tangential resolutions. Compensating for this reduction is feasible by increasing axial samplings [6,27–29]. CBM mode is particularly efficient for scans exceeding a single BP,

Table 2
A comparison of the uniformity, spillover ratio (SORs), and recovery coefficients (RCs) measurements, was evaluated using the image quality (IQ) phantom for both S&S and CBM acquisition modes.

	Uniformity				SORs				RCs				
	Mean	Max	Min	STD (%)	Water hole	STD (%)	Air hole	STD (%)	1 (mm)	2 (mm)	3 (mm)	4 (mm)	5 (mm)
CBM mode	0.029	0.048	0.017	4.52	0.32	3.18	0.31	3.16	0.17	0.43	0.68	0.89	0.93
S&S mode	0.028	0.043	0.019	4.35	0.31	3.15	0.34	3.43	0.15	0.48	0.71	0.88	0.91

emphasizing sensitivity or reducing scan duration, as in dynamic WB imaging.

In CBM mode (OS-50 %), scan time reductions of approximately 30–60 % for 1–4 BPs compared to S&S(MRD-9) mode are feasible while maintaining similar absolute sensitivity. This reduction is particularly valuable for dynamic WB imaging. In dynamic imaging procedures, the flexibility of CBM mode allows for acquiring more passes within a constant scan time or longer scan times per pass, enhancing sensitivity and image quality. Sensitivity declines with increased BM speed in CBM mode, posing a trade-off between sensitivity and scan time (Fig. 4). The 'equivalent speed' in CBM mode, compared to S&S(WO-MRD), is around 0.14 mm s^{-1} and varies from 0.21 to 0.3 mm s^{-1} compared to S&S(MRD-9) mode (Fig. 5). This variation is due to differences in absolute sensitivity and scanning overlapping areas between consecutive BPs in S&S mode. Selection of the equivalent speed is crucial to maintain consistent sensitivity across CBM and S&S modes, although the bed speed in CBM mode may vary depending on the imaging procedure.

The study evaluated the Xtrim-PET scanner's performance in CBM (OS-5 %) mode versus S&S(MRD-9) mode based on the NEMA standard. It found no significant changes in radial and tangential resolutions but observed an 11 % decline in axial resolution in CBM mode, attributable to random coincidences detected across all rings. This decrease can be mitigated by increasing axial sampling [6]. Table 3 highlights the resolution's dependence on crystal size, with smaller sizes yielding better resolution. The Xtrim's resolution in both data acquisition modes, is well comparable against other scanners within the same category (close AFOV and TAFOV dimensions), which have resolutions ranging from 1.08 mm (IRIS XL-220 [25]) to 2.6 mm (SAFIR [26]). In CBM(OS-50 %) mode, absolute system sensitivity increased by 26 % compared to S&S (MRD-9) mode, owing to MRD application. The peak absolute sensitivities of Xtrim for CBM and S&S modes were 1.6 % and 2.9 %, respectively. Compared to other scanners, they have a peak absolute sensitivity of 1.06 % (SAFIR [26]) to 4.32 % (Argus [18]), suggesting efficient sensitivity of the Xtrim for small-animal imaging. The study also noted a transition in sensitivity profile shape post-MRD application, enhancing the importance of absolute system sensitivity. NECR values showed minimal variation between CBM and S&S(WO-MRD) modes, indicating no significant changes. The NECR values of Xtrim in both data acquisition modes are comparable against scanners in the same category, ranging from 16.9 kcps (Albira 1ring [22]) to 897 kcps (microPET Focus-120 [19]) for the mouse, and from 12.8 kcps (Albira [22]) to 267 kcps (Focus-120 [19]) for the rat. SF values remained consistent across both modes. The SF in Xtrim compares well with other scanners, with SF values ranging from 5.6 % (Focus-120 [19]) to 21 % (Argus [18]) for mouse and from 10 % (IRIS XL-220 [25]) to 34.4 % (Argus [18]) for rat. Image quality parameters showed no significant alteration, with CV values of uniformity reduced in CBM mode due to higher sensitivity at scan length extremes. Overall, the Xtrim's image quality parameters compared favorably to similar scanners.

The analysis reveals that in CBM(OS-50 %) mode, absolute system sensitivity decreases by 4.9 % to 8.1 % compared to S&S(MRD-9) mode, but relative to CBM(WO-MRD) mode, it increases by 37.9 % to 42.7 %. Despite reduced sensitivity, CBM mode shows scan time reductions of 1.9 %, 7.7 %, and 10.7 % for scan lengths of 2, 3, and 4 BPs, respectively, compared to CBM(WO-MRD) mode. The slight reduction in total scan time in CBM mode is due to overlapping scan areas (21 %) and BM time. Moreover, CBM mode offers significant scan time reductions of 47.8 %, 54.8 %, and 58.3 % for 2, 3, and 4 BPs scans, respectively, relative to S&S(MRD-9) mode, facilitating dynamic WB imaging. This reduction enables more passes in CBM mode than in S&S mode within a fixed total scan time, crucial for dynamic imaging. This approach allows for generating SUV and parametric images concurrently, offering

Table 3
Design Characteristics and NEMA performance measurement for preclinical PET scanners.

Scanner (Reference)	Scintillator (Arrays) Electronic	Crystal Dimensions (mm^3)	TFOV AFOV (mm)	TW (ns) ER (%)	Resolution (mm) Radial FWHM [Reconstruction]	Peak Absolute Sensitivity (%) (EW)	NECR (kcps) Mice Rat	SF (%) Mice Rat
Micro-PET R4 [17]	LSO (8 × 8) PSPMT	2.1 × 2.1 × 10	100 78	6 23	2.13 at 5 mm FORE + FBP	2.06 (350–650)	618 164	9.3 22.2
Argus (eXplore Vista) [18]	LYSO/GSO (13 × 13 / 20 × 20) PSPMT	1.45 × 1.45 × 7 / 8	67 68	7 26 / 33	1.63 at 5 mm 2D FBP	4.32 (250–700)	117 40	21 34.4
microPET Focus-120 [19]	LSO (12 × 12) PSPMT	1.51 × 1.51 × 10	100 76	6 18.3	1.92 at 5 mm FORE + FBP	3.42 (350–650)	897 267	5.6 20.3
VrPET [20]	LYSO (30 × 30) PSMPT	1.4 × 1.4 × 12	86.6 45.6	3.8 16.5	1.52 at 5 mm SSRB + FBP	2.22 (100–700) 1.56 (250–650)	74 (100–700) 31	11.5 23.3
LabPET8 [21]	LYSO/LGSO APD	2 × 2 × 11.9 / 13.3	100 75	20 24 / 25	1.65 at 5 mm SSRB + FBP	2.36 (250–650)	279 94	15.6 29.5
Albira 1 ring [22]	LYSO MAPMT	50 × 50 × 10	80 46	5 18	1.65 at 5 mm SSRB + FBP	2.5 (255–767) 2.0 (358–664)	16.9 (358–664) 12.8	7.5 13
TransPET-LH [23]	LYSO PSPMT	1.89 × 1.89 × 13	130 53	5 13	0.95 at center 3D OSEM	2.4 (250–750) 2.04 (350–650)	110 (250–750) 40	11 19.3
Trans-PET/CT X5 [24]	LYSO (13 × 13) NA	1.9 × 1.9 × 13	130 50	5 15	2.11 at center SSRB + FBP	1.7 (350–650)	126 61	14 24
Xtrim-PET [14]	LYSO (24 × 24) SiPMs	2.1 × 2.1 × 10	100 50.4	5 12	2.01 at 5 mm SSRB + FBP	2.99 (250–650) 2.2 (400–700)	113.2 (250–650) 82.8	12.5 25.8
IRIS XL-220 PET/CT [25]	LYSO (27 × 27) MAPMT	1.6 × 1.6 × 16	170 45	5.2 NA	1.08 – FBP 0.89– 3D OSEM at center	2.81 (250–750) 2.37 (400–620)	NP 88 (400–620)	NP 10
SAFIR PET/MR [26]	LYSO (8 × 7 / 8) SiPMs	2.1 × 2.1 × 13	90 35.6	0.5 13.8	2.6 at 5 mm FBP3DRP	1.06 (391–601)	799 121	10.9 17.8
Xtrim-PET CBM (2023) [This study†]	LYSO (24 × 24) SiPMs	2.1 × 2.1 × 10	100 Optional	5 12	1.95 at 5 mm SSRB + FBP	1.6 (250–650)	117.8 (250–650) 85.6	12.8 26.4

Abbreviations: FBP: Filtered Back Projection, FORE: Fourier Rebinning, NA: Not Available, NP: Not Performed, OSEM: Ordered Subset Expectation Maximization, PMT: Photomultiplier Tube, PSPMT: Position Sensitive PMT, SSRB: Single Slice Rebinning.

† The outcome of the NEMA NU4 performance evaluation performed on the Xtrim-PET scanner utilizing the CBM acquisition mode.

complementary information for medical professionals [30,31]. In addition to the advantages mentioned above, of imaging with CBM mode – such as increased absolute system sensitivity, shorter scan time, and improved uniformity of sensitivity profile – there are numerous other key advantages. In imaging with CBM mode, the scan length can be set as desired, unlike the S&S mode, which restricts to a few BP selections. Moreover, a shorter scan time is required for a fixed scan length, which is crucial for dynamic imaging. In general, CBM mode is ideally preferred for scanning an extended region (multiple BPs). In cases where the ROI can be covered via the AFOV, it is recommended to perform a single BP scan with S&S mode.

5. Conclusion

The employment of CBM mode provides a versatile and efficient approach for rapid whole-body static and dynamic data acquisition in small-animal PET scanners with a limited AFOV. This study aimed to specifically optimize the CBM data acquisition mode for small-animal PET scanners, with a primary focus on its applicability for WB imaging purposes. Following the optimization process, the resulting mode was successfully implemented on the preclinical Xtrim-PET scanner. The findings of this study indicated that the CBM mode exhibits high absolute system sensitivity and, also generates a uniform axial sensitivity profile, leading to more uniform images. Consequently, WB CBM PET scans display a more consistent axial noise profile across varying BPs and offer a customizable total axial length. However, using CBM acquisition with matched S&S sampling causes a slight degradation in axial resolution. On the contrary, enhancing the axial sampling has the potential to ameliorate this, as was seen in the measurements of axial resolution. In this regard, CBM protocols enable uninterrupted data acquisition in the z-direction, encompassing WB coverage, thus eliminating the necessity for the acquisition of partially redundant PET data due to FOV overlap between consecutive bed positions. The differences as mentioned earlier between both acquisition modes confer several benefits to the CBM, including enhanced efficiency in protocol setup, and the capability to execute intricate protocols in a single pass, and within a time that aligns well with routine preclinical usage. The implementation of CBM necessitated only minimal modifications to the system hardware. As such, the system's reliability depends on the precision of the acquisition time and the requested bed speed, which determines the bed's positioning throughout the scan.

Declaration of competing interest

The authors declare that they have no known competing financial interests or personal relationships that could have appeared to influence the work reported in this paper.

Acknowledgements

The authors would like to extend their gratitude to the personnel at Parto Negar Persia Co., and the Radiation Research Centre at Shiraz University for their valuable assistance and support. This work partially supported through grant No. 41652 from the Tehran University of Medical Sciences. Additionally, the authors would like to acknowledge and express their appreciation for the generous financial assistance extended by Tehran University of Medical Sciences and Shiraz University. Their generous funding played a vital role in facilitating the completion of this research endeavor.

References

[1] Miyaoka RS, Lehnert AL. Small animal PET: a review of what we have done and where we are going. Phys Med Biol 2020;65:24TR04..
[2] Amirrashedi M, Zaidi H, Ay MR. Advances in preclinical PET instrumentation. PET clinics 2020;15:403–26.
[3] Goertzen AL, Bao Q, Bergeron M, Blankemeyer E, Blinder S, Cañadas M, et al. NEMA NU 4–2008 comparison of preclinical PET imaging systems. J Nucl Med 2012;53:1300–9.
[4] Du J, Jones T. Technical opportunities and challenges in developing total-body PET scanners for mice and rats. EJNMMI physics 2023;10:1–28.
[5] Hu J, Panin V, Smith AM, Spottiswoode B, Shah V, von Gall CC, et al. Design and implementation of automated clinical whole body parametric PET with continuous bed motion. IEEE Transactions on Radiation and Plasma Medical Sciences 2020;4:696–707.
[6] Panin V, Smith A, Hu J, Kehren F, Casey M. Continuous bed motion on clinical scanner: design, data correction, and reconstruction. Phys Med Biol 2014;59:6153.
[7] Guo X, Wu J, Chen M-K, Liu Q, Onofrey JA, Pucar D, et al. Inter-Pass Motion Correction for Whole-Body Dynamic PET and Parametric Imaging. IEEE Transactions on Radiation and Plasma Medical Sciences 2022;7:344–53.
[8] Panin V, Smith A, Casey M. In: Normalization coefficient computing for continuous bed motion acquisition. NSS/MIC): IEEE; 2013. p. 1–10.
[9] Alberts I, Hünermund J-N, Prenosil G, Mingels C, Bohn KP, Viscione M, et al. Clinical performance of long axial field of view PET/CT: a head-to-head intra-individual comparison of the Biograph Vision Quadra with the Biograph Vision PET/CT. Eur J Nucl Med Mol Imaging 2021;48:2395–404.
[10] Karakatsanis NA, Garibotto V, Rager O, Zaidi H. Continuous bed motion Vs. step-and-shoot acquisition on clinical whole-body dynamic and parametric PET imaging. In: 2015 IEEE Nuclear Science Symposium and Medical Imaging Conference (NSS/MIC): IEEE; 2015. p. 1–6.
[11] Osborne DR, Acuff S. Whole-body dynamic imaging with continuous bed motion PET/CT. Nucl Med Commun 2016;37:428.
[12] Association NEM. Performance measurements of small animal positron emission tomographs. NEMA Standards. Publication 2008,;NU4-2008:1–23.
[13] Sajedi S, Zeraatkar N, Taheri M, Kaviani S, Khanmohammadi H, Sarkar S, et al. Development and preliminary results of Xtrim-PET, a modular cost-effective preclinical scanner. Nucl Instrum Methods Phys Res, Sect A 2019;940:288–95.
[14] Amirrashedi M, Sarkar S, Ghafarian P, Hashemi Shahraki R, Geramifar P, Zaidi H, et al. NEMA NU-4 2008 performance evaluation of Xtrim-PET: A prototype SiPM-based preclinical scanner. Med Phys 2019;46:4816–25.
[15] Santin G, Strul D, Assié K, Autret D, Avner S, Barbier R, et al. GATE: a simulation toolkit for PET and SPECT. Phys Med Biol 2004;49:4543.
[16] Siman W, Kappadath SC. Comparison of step-and-shoot and continuous-bed-motion PET modes of acquisition for limited-view organ scans. J Nucl Med Technol 2017;45:290–6.
[17] Knoess C, Siegel S, Smith A, Newport D, Richerzhagen N, Winkeler A, et al. Performance evaluation of the microPET R4 PET scanner for rodents. Eur J Nucl Med Mol Imaging 2003;30:737–47.
[18] Wang Y, Seidel J, Tsui BM, Vaquero JJ, Pomper MG. Performance evaluation of the GE healthcare eXplore VISTA dual-ring small-animal PET scanner. J Nucl Med 2006;47:1891–900.
[19] Kim JS, Lee JS, Im KC, Kim SJ, Kim S-Y, Lee DS, et al. Performance measurement of the microPET focus 120 scanner. J Nucl Med 2007;48:1527–35.
[20] Lage E, Vaquero JJ, Sisniega A, España S, Tapias G, Udías Á, et al. VrPET/CT: Development of a rotating multimodality scanner for small-animal imaging. In: 2008 IEEE Nuclear Science Symposium Conference Record: IEEE; 2008. p. 4671–4.
[21] Prasad R, Ratib O, Zaidi H. NEMA NU-04-based performance characteristics of the LabPET-8™ small animal PET scanner. Phys Med Biol 2011;56:6649.
[22] Balcerzyk M, Kontaxakis G, Delgado M, Garcia-Garcia L, Correcher C, Gonzalez AJ, et al. Initial performance evaluation of a high resolution Albira small animal positron emission tomography scanner with monolithic crystals and depth-of-interaction encoding from a user's perspective. Meas Sci Technol 2009;20:104011.
[23] Wang L, Zhu J, Liang X, Niu M, Wu X, Kao C-M, et al. Performance evaluation of the Trans-PET® BioCaliburn® LH system: a large FOV small-animal PET system. Phys Med Biol 2014;60:137.
[24] Teuho J, Han C, Riehakainen L, Honkaniemi A, Tirri M, Liljenbäck H, et al. NEMA NU 4–2008 and in vivo imaging performance of RAYCAN trans-PET/CT X5 small animal imaging system. Phys Med Biol 2019;64:115014.
[25] Boisson F, Serriere S, Cao L, Bodard S, Pilleri A, Thomas L, et al. Performance evaluation of the IRIS XL-220 PET/CT system, a new camera dedicated to non-human primates. EJNMMI physics 2022;9:1–14.
[26] Khateri P, Lustermann W, Ritzer C, Tsoumpas C, Dissertori G. NEMA characterization of the SAFIR prototype PET insert. EJNMMI physics 2022;9:1–15.
[27] Chatziioannou A, Dahlbom M. Study of the effects of whole body PET spatial sampling schemes on data SNR. In: 1996 IEEE Nuclear Science Symposium Conference Record: IEEE; 1996. p. 1295–9.
[28] Dahlbom M, Chatziioannou A, Hoh CK. Resolution characterization of continuous axial sampling in whole body PET. In: 1995 IEEE Nuclear Science Symposium and Medical Imaging Conference Record: IEEE; 1995. p. 1011–5.
[29] Townsend DW, Reed J, Newport DF, Carney JP, Tolbert S, Newby D, et al. Continuous bed motion acquisition for an LSO PET/CT scanner. In: IEEE Symposium Conference Record Nuclear Science 2004: IEEE; 2004. p. 2383–7.
[30] Zhou C, Luk WK, Casey ME. Summing of dynamic sinograms. In: 2015 IEEE Nuclear Science Symposium and Medical Imaging Conference (NSS/MIC): IEEE; 2015. p. 1–4.
[31] Karakatsanis NA, Casey ME, Knesaurek K, Fayad ZA, Kostakoglu L. SUV/Patlak-4D whole-body PET/CT dynamic and parametric imaging: clinical demonstration and validation of SUV synthesis from dynamic passes. In: 2017 IEEE Nuclear Science Symposium and Medical Imaging Conference (NSS/MIC): IEEE; 2017. p. 1–6.